A Compact Tri-Band Frequency Reconfigurable Antenna for LTE/Wi-Fi/ITS Applications

Shreyas S. Bharadwaj[1], Deepika Sipal[2], Dinesh Yadav[1, *], and Shiban K. Koul[2]

Abstract—In this work, a Tri-Band frequency reconfigurable antenna for LTE (Long Term Evolution)/WiFi (Wireless Fidelity)/ITS (Intelligent Transportation Systems) applications is presented. The proposed design consists of a wine glass shaped slotted radiating patch along with a switchable rectangular ring type slot on the ground plane. This structure operates in three different states viz. state-1, state-2, and state-3 at 4.5 GHz (LTE band), 5.9 GHz (ITS band), and 3.8 GHz (LTE band)/5 GHz (Wi-Fi band), respectively, with an overall compact size of $30 \times 30 \times 0.762 \, \text{mm}^3$. Multi-band resonances are obtained by incorporating slots in the main radiating element and ground plane. Moreover, switching among these bands is achieved by placing two PIN diodes at optimized positions on the rectangular ring slot in the ground plane. For the proposed design, good agreement between simulated and measured results is obtained in all the three operating states of the design, which makes it suitable for compact reconfigurable systems.

1. INTRODUCTION

The quick and continuous technological expansion of modern communication keeps demanding smarter and more compliant, condensed, and handy wireless devices. Thus, antennas in modern wireless devices must adapt to changing system requirements in different environments and adapt to changing system requirements. Incorporation of reconfigurability in antenna designs has been considered as one of the solutions to meet the requirements of the modern wireless system as a prudent solution [1]. Easy integration with control circuits and smaller size have always given reconfigurable antennas an edge over fixed-tuned antennas. Therefore, research on compact multi-band reconfigurable antennas has attracted significant attention lately [2–6]. Structures that combine two independent antennas operating in different frequency bands with a single feed that can perform efficient switching and tuning between two or more operating bands have been discussed in [2–4]. In the literature, different slotted structures have been reported which resonate at one or more frequency bands [5–9]. In [7], the antenna resonates at three frequency bands; however, it is not suitable for compact devices due to its large size (65 mm × 80 mm). In [8], a compact antenna (30 mm × 35 mm) has been presented for three frequency bands; however, the design does not show frequency reconfigurability, which limits its performance. A dual-band antenna with characteristics to switch among WLAN frequencies has been discussed in [9]; however, the antenna can switch among WLAN frequency bands only.

Therefore, in this communication, a frequency reconfigurable compact monopole antenna with a simple structure is proposed. The proposed antenna switches among three frequency states with the use of two PIN diodes. The compact design of the antenna makes it useful for different applications such as LTE (Long Term Evolution)/WiFi (Wireless Fidelity)/ITS (Intelligent Transportation Systems) applications. In the following sections, the proposed design is discussed in detail. Section 2 discusses

* Corresponding author: Dinesh Yadav (dineshyadav_1984@yahoo.co.in).
[1] Department of Electronics & Communication Engineering, Manipal University Jaipur, Rajasthan, India. [2] Centre for Applied Research in Electronics (CARE), Indian Institute of Technology (IIT) Delhi, Hauz Khas, New Delhi, India.

its geometry, and Section 3 presents its working mechanism and parametric analysis. Moreover, finally, all the simulated results are verified by the measurement in Section 4.

2. GEOMETRY OF THE PROPOSED MULTIBAND ANTENNA

Figure 1 illustrates the optimized top and bottom views of the proposed antenna. The dimensions of the overall structure are $30\,\text{mm} \times 30\,\text{mm}$, and the antenna is fabricated on a Neltec substrate (dielectric constant '$\varepsilon_r' = 3.2$, loss tangent '$\tan\delta' = 0.0024$, dielectric thickness '$h' = 0.762\,\text{mm}$). The simulations are obtained using Computer Simulation Technology — Microwave Studio (CST-MWS). The antenna structure consists of triangular radiating patch in which two slots were inserted of the size $WS3 \times LS3$ each. A rectangular ring slot is cut at bottom plane of the antenna to achieve re-configurability by placing two diodes $D1$ and $D2$ through three biasing states. The biasing circuit of the diode is placed on the top side of the antenna comprises of RF-choke inductor, biasing pads as shown in Fig. 1(a). Optimization of the parameters is performed using CST Microwave Studio and are listed in Table 1.
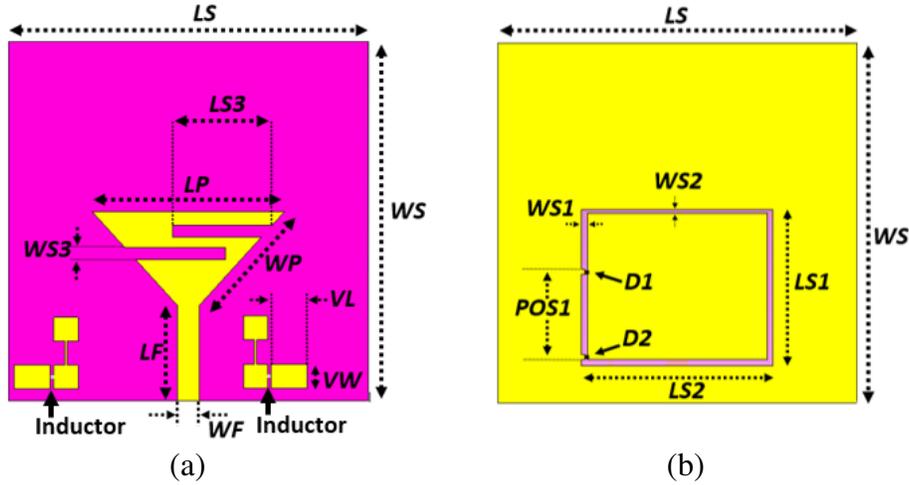

(a)   (b)

Figure 1. Geometry of the proposed reconfigurable antenna, (a) top view and (b) bottom view. (Yellow color represents copper, and pink color represents dielectric).

Table 1. Optimized values of the structural parameters of reconfigurable antenna.

Parameter	Size (mm)	Parameter	Size (mm)	Parameter	Size (mm)
LS	30	$WS2$	0.3	LF	8
WS	30	$LS3$	8.3	WF	1.8
$LS1$	13	LP	16	$POS1$	7.3
$LS2$	16	$WS3$	1.35	VL	3
$WS1$	0.5	WP	10.53	VW	2

3. WORKING MECHANISM AND PARAMETRIC ANALYSIS

3.1. Working Mechanism

The proposed design operates in three states listed in Table 2. Switching among three operating states is carried out using two PIN diodes (MA4SPS552) named as D1 and D2 shown in Fig. 1. These diodes are placed in the rectangular ring slot at the optimum position on the ground plane. The equivalent circuit of the diode in ON and OFF states is shown in Fig. 2(a). The biasing circuit of the diode is

Table 2. Operating states of the proposed antenna.

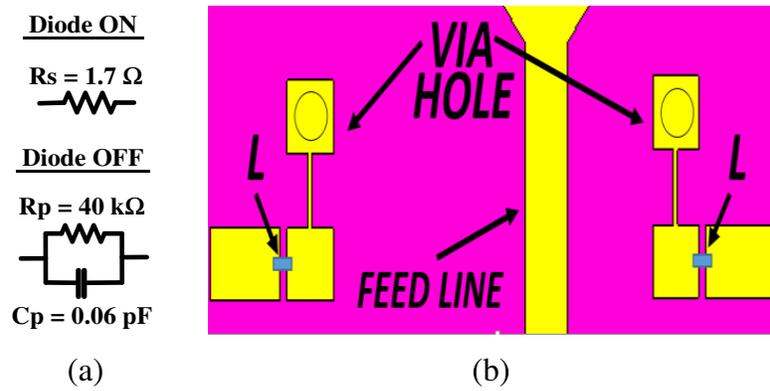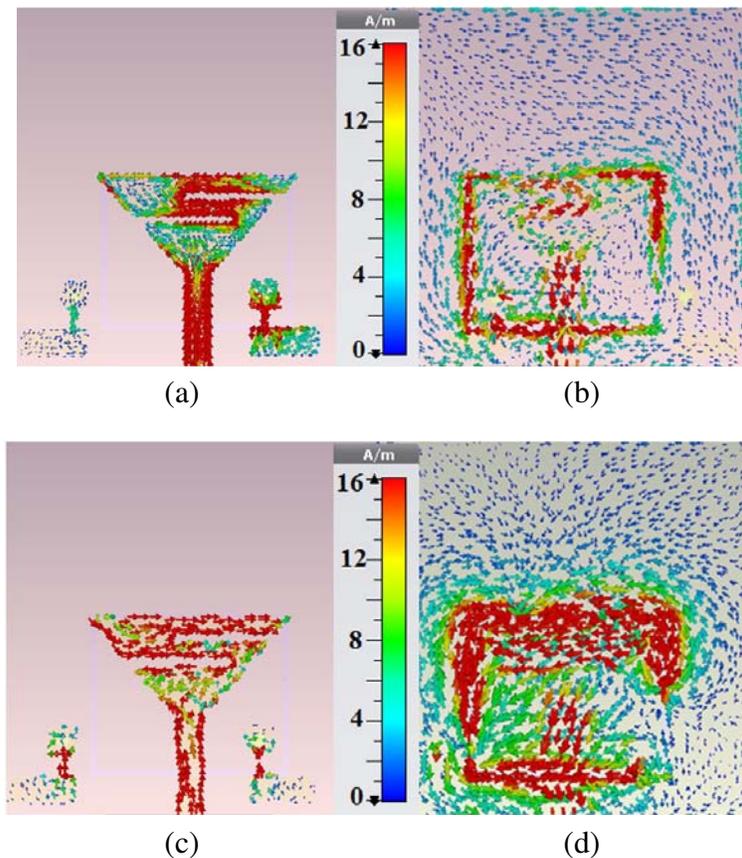| OPERATING STATES	DIODE STATE	FREQUENCY (GHz)	BANDWIDTH (GHz)
STATE-1	D1 OFF, D2 OFF	4.5	0.79
STATE-2	D1 ON, D2 OFF	5.9	0.1
STATE-3	D1 OFF, D2 ON	3.8	0.33
		5	0.62

Figure 2. (a) Equivalent circuit of the diode in ON and OFF states, (b) DC biasing circuit of the proposed antenna where L is an inductor.
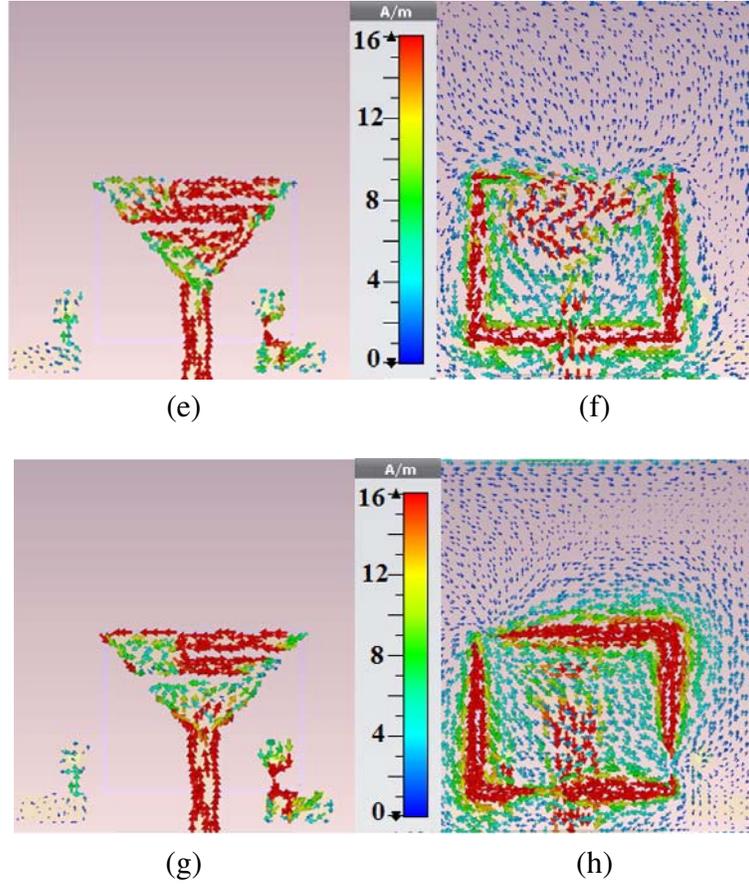
Figure 3. Simulated surface current characteristics of the proposed antenna at various frequencies and different diode states: (a) and (b) state-1, (c) and (d) state-2, (e), (f), (g) and (h) state-3. (a) Top view at 4.5 GHz, (b) bottom view at 4.5 GHz, (c) top view at 5.9 GHz, (d) bottom view at 5.9 GHz, (e) top view at 3.8 GHz, (f) bottom view at 3.8 GHz, (g) top view at 5 GHz, (h) bottom view at 5 GHz.

placed on the top side of the antenna for easy integration of the components, as shown in Fig. 2(b). The biasing circuit of each diode consists of RF choke inductor of value 100 nH. The same biasing circuit is used to switch ON and OFF the diode D1 and D2. This is achieved due to the complementary placement of the diodes; therefore, when the diode D1 is ON, D2 will be OFF, and when the diode D2 is ON, D1 will be OFF. This arrangement of diodes makes the design very simple and compact.

For understanding the working mechanism of the proposed antenna, the simulated surface current distribution is investigated in Fig. 3. In state-1, when D1 and D2 are OFF, the inner and the outer rectangular structures in the ground plane are separated from each other; as a result of this, the coupling between the main radiating element and ground plane is reduced. In this state, the current concentrates along the slots in the top radiator from mid-point of the upper slot to mid-point of the lower one, traversing total path length of 15.35 mm which is approximately equal to $\lambda 1/4$ ($\lambda 1$ is the wavelength corresponding to central frequency at 4.5 GHz) which allows the antenna to operate in the 4.5 GHz band, i.e., state-1. In state-2, when only D1 is ON and D2 is OFF, a 'short-circuit' path in-between the two rectangular ground plane structures is achieved; which results in more coupling between the radiator and the ground plane as shown in Figs. 3(c) and (d) as compared to Figs. 3(a) and (b). In this state, the current concentration is higher near the upper edge of the ground slot, starting from the middle of side $LS1$, to the point where D1 is placed constituting about 26 mm or $\lambda 2/2$ ($\lambda 2$ is the wavelength corresponding to center frequency at 5.9 GHz) which makes the current travel through a smaller path and corresponding resonance is achieved in 5.9 GHz, i.e., state-2. In state-3, when only D2 is ON, and D1 is OFF, the coupling between radiator and ground plane is shown in Figs. 3(e) and (f).

The surface current concentration shows that the current travels through a length of 39.4 mm, which is approximately $\lambda 3A/2$ ($\lambda 3A$ is the wavelength corresponding to center frequency at 3.8 GHz). The total path traveled by the surface current is along the left, right, and bottom parts of the rectangular ring slot in the ground plane, which introduces resonance at 3.8 GHz, i.e., state-3. Apart from this frequency in state-3, the surface current travels through a shorter path along the top right corner and bottom left corner of the rectangular ring slot in the ground plane by covering a distance of 15.2 mm which is approximately equal to $\lambda 3B/4$ ($\lambda 3B$ is the wavelength corresponding to center frequency at 5 GHz) and is responsible for the resonance at 5 GHz. The above analysis of the surface current distribution of the proposed antenna at the respective operating frequency clearly shows that the individual part of the antenna is responsible for resonance at a particular frequency. This analysis also shows the effects of ON and OFF states of the diodes.

3.2. Parametric Analysis

In this section, parametric analysis of the main parameters of the proposed antenna is presented, which mainly affects the resonance frequency band of the antenna. The first one is the width of the gap on the left side of the rectangular ring slot on the ground plane, i.e., $WS1$, and the second one is a vertical shift in the position of the diode along the left side of the rectangular ring slot, i.e., $POS1$.

The parametric analysis is performed on the antenna to show the frequency reconfiguration property of the proposed antenna. For analysis of the effect of both the parameters, i.e., $WS1$ and $POS1$, on the performance of the antenna, only one parameter is varied, and all the others remain uninterrupted.

3.2.1. Gap Width (WS1)

Figure 4 shows the return loss of the antenna for different values of $WS1$. As $WS1$ increases, the lower frequency of the operating band shifts towards the upper side, thereby reducing the operating bandwidth of the antenna from approximately 800 MHz to 400 MHz. At the same time, with an increase in the value of $WS1$, the impedance matching improves till $WS1 = 1$ mm; however, from $WS1 = 1$ mm to 1.5 mm, the impedance matching seems to reduce but remains below -10 dB.
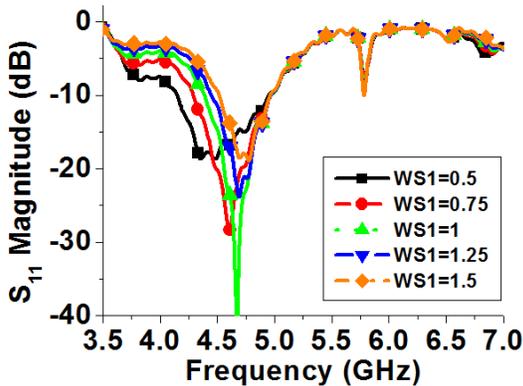

Figure 4. Effect of increasing the gap width ($WS1$) of the rectangular ring slot on the reflection coefficient.
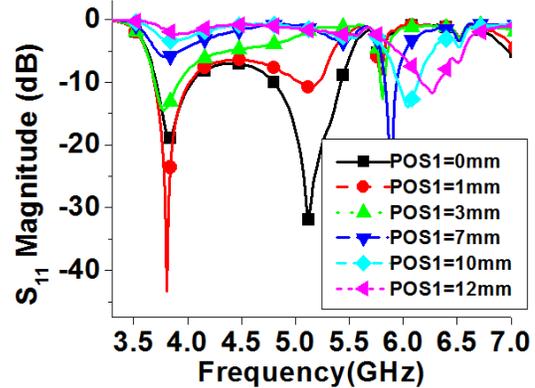
Figure 5. Effect of upward shifting of the position of the diode ($POS1$) on the reflection coefficient.

3.2.2. Diode Position (POS1)

Figure 5 shows the return loss characteristics of the antenna for different diode positions along the vertical slot of the rectangular ring slot in the ground plane. The position of the diode ($POS1$) along the vertical slot is varied from 0 mm to 12 mm. When $POS1 = 0$ mm, the antenna resonates in dual frequency bands, 3.8 GHz and 5 GHz, because the total length traveled by the surface currents provides resonance at these frequencies as shown in Figs. 3(f) and (h). As $POS1$ is increased from 1 mm to

7 mm, it is observed that the dual band resonance at the lower band is slowly eliminated. However, at $POS = 7$ mm, it is totally eliminated while introducing another resonance band at 5.9 GHz. The resonance at 5.9 GHz shifts towards the higher side and also improves the bandwidth with an increase in the value of $POS1$ from 7 mm to 12 mm.

From the parametric analysis, it is concluded that there is a tradeoff between the frequency and bandwidth. Therefore, for the proposed design to achieve desired operating frequency and bandwidth, the optimum values of these two parameters are as follows; $WS1 = 0.5$ mm, $POS1 = 0$ mm for D2, and $POS1 = 7.3$ mm for D1.

4. RESULTS AND DISCUSSIONS

The prototype has been fabricated on a copper clad Neltec substrate, and its photographs are shown in Fig. 6. This prototype is fabricated using the standard process of photolithography, which consists of three basic steps: printing the design on a mask, using a radiation-sensitive material to transfer the layout to the substrate, and finally etching the unwanted area with the use of chemicals. This fabrication technique is cost-effective. The fabricated design is measured for verification of its S-parameter. The measured S-parameters are obtained using Anritsu Vector network analyzer. The simulated and measured return loss characteristics are shown in Fig. 7. The simulated and measured impedance bandwidths ($S_{11} < -10$ dB) are of the order of 17.8% in state-1 (from 4.14–4.94 GHz), 1.87% in state-2 (from 5.83–5.94 GHz), 8.63% in state-3 (from 3.70–4.03 GHz), and 12.3% in state-3 (from 4.78–5.41 GHz). The measured results in state-3 are slightly deviated as compared to the simulated values. This anomaly can be attributed to the tolerances of the fabricated antenna structure as well as measurement uncertainties.
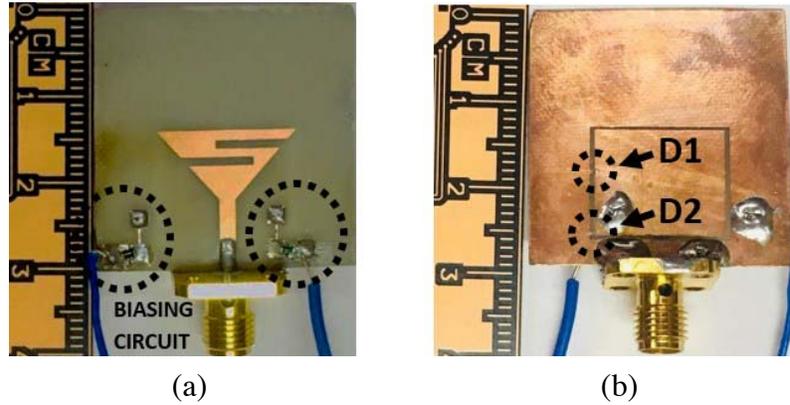

(a)   (b)

Figure 6. Fabricated prototype of the proposed antenna, (a) top view and (b) bottom view.

Table 3. Comparison between literature and proposed antenna.

Ref No	OB* (GHz)	N*	S*	Size (λ)	Diode Type
[10]	0.9, 1.7	4	4	$0.5\lambda \times 0.5\lambda \times 0.004\lambda$	PIN
[11]	2, 4.5, 5.2	2	4	$0.47\lambda \times 0.37\lambda \times 0.02\lambda$	PIN
[12]	0.9, 1.8, 2.4, 2.1, 1.5	2	4	$0.31\lambda \times 0.21\lambda \times 0.004\lambda$	PIN
[13]	2.42, 2.36, 3.64	1	2	$0.5\lambda \times 0.25\lambda \times 0.008\lambda$	PIN
[14]	1.8–3.4	4	Continuous	$0.4\lambda \times 0.8\lambda \times 0.012\lambda$	Varactor
[15]	3.3–7	4	Continuous	$0.44\lambda \times 0.5\lambda \times 0.021\lambda$	Varactor
This work	3.8, 4.5, 5, 5.9	2	3	$0.37\lambda \times 0.37\lambda \times 0.008\lambda$	PIN

Note: $OB* =$ Operating Band, $N* =$ Number of diodes and $S* =$ Number of states
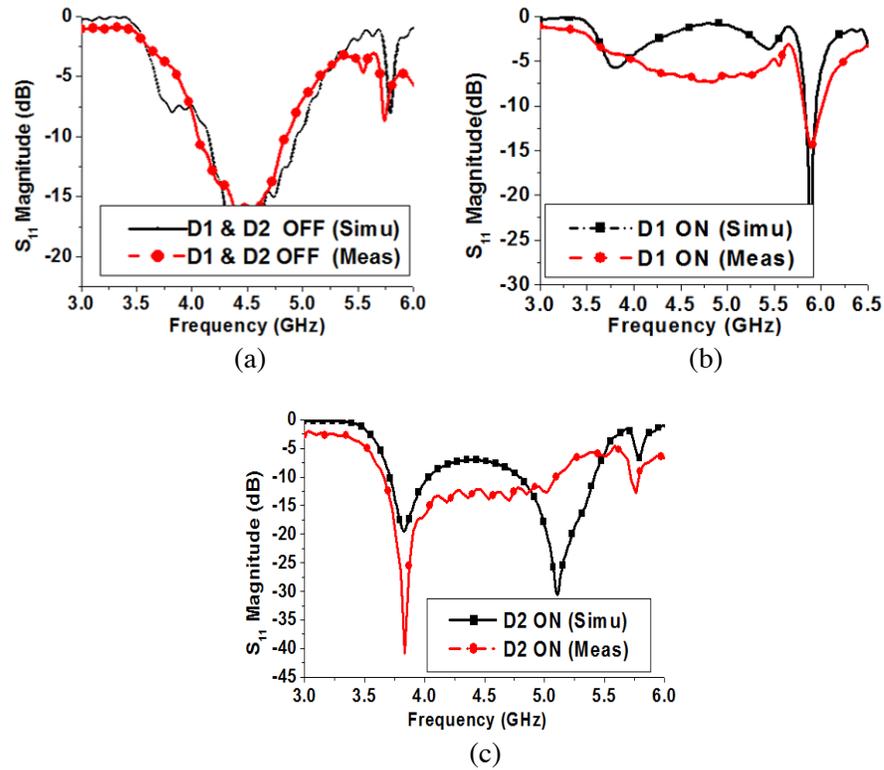
Figure 7. Simulated and measured reflection coefficient for the proposed antenna in (a) state-1, (b) state-2 and (c) state-3.
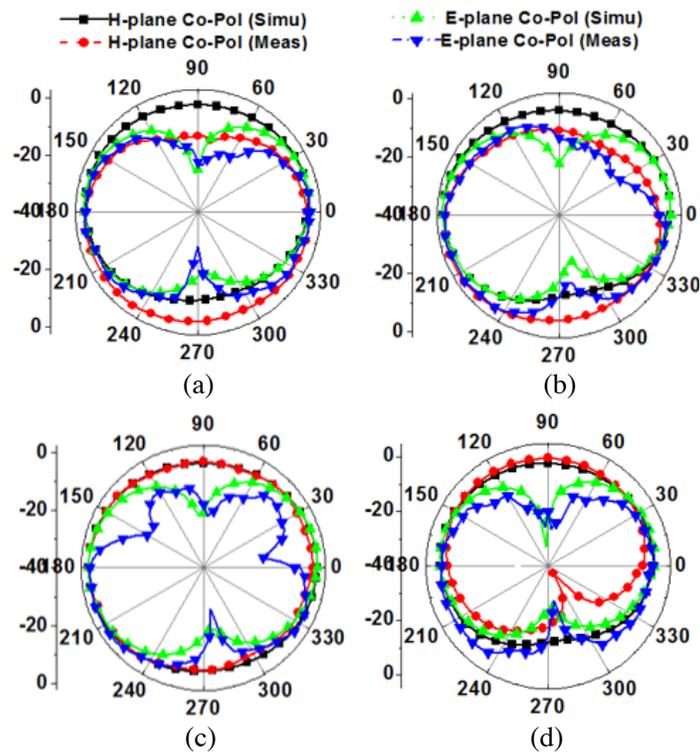

Figure 8. Measured and simulated far field gain patterns in (a) state-1 at 4.5 GHz, (b) state-2 at 5.9 GHz, (c) state-3 at 3.8 GHz, (d) state-3 at 5 GHz.
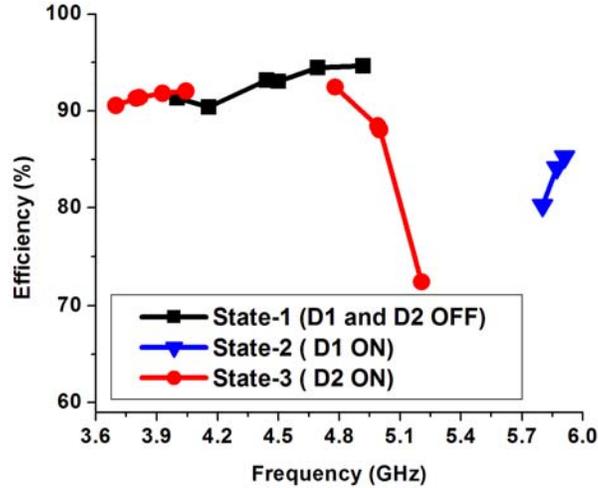
Figure 9. Simulated radiation efficiency of the antenna in various diode states.

The simulated and measured normalized far-field gain patterns at 4.5 GHz, 5.9 GHz, 3.8 GHz, and 5 GHz of the proposed antenna are presented in Fig. 8. It is observed that the measured results are in good agreement with the simulated ones. In the simulation, the gain at 4.5 GHz, 5.9 GHz, 3.8 GHz, and 5 GHz is 3.9 dBi, 4.64 dBi, 3.31 dBi, and 3.8 dBi, respectively, which indicates that the proposed antenna operates ol/.ver the resonating frequencies with gain larger than 3.31 dBi. The measured gains of the proposed antenna are 2.82 dBi, 3.93 dBi, 1.95 dBi, and 2.45 dBi at the respective frequencies. The radiation efficiencies of the antenna in State-1, State-2, and State-3 are observed to be more than 90%, 80%, and 73% respectively as shown in Fig. 9.

Table 3 compares recent work in the literature with the proposed antenna. The vital features of the presented design are attributed to its compact design along with its ability to cover three different frequency bands (two single bands and one dual band) with only two integrated PIN diodes.

5. CONCLUSION

This paper presents a frequency reconfigurable tri-band antenna by using two PIN diodes. The antenna can be used in LTE (Long Term Evolution)-band, ITS (Intelligent Transportation Systems)-band or Wi-Fi (Wireless Fidelity) and LTE-band depending upon user's requirements. The impedance bandwidths achieved are 17.8%, 1.87%, 1.63%, and 12.3% in the three states of the proposed antenna. Moreover, the maximum gain of the antenna reaches 4.64 dBi. The proposed frequency reconfigurable multi-band antenna is promising for adaptive wireless communication applications such as intelligent vehicle communication systems and others.

REFERENCES

1. Ciccia, S., G. Giordanengo, S. Arianos, F. Renga, P. Ruiu, A. Scionti, L. Mossucca, O. Terzo, and G. Vecchi, "Reconfigurable antenna system for wireless applications," *IEEE 1st International Forum on Research and Technologies for Society and Industry Leveraging a Better Tomorrow (RTSI)*, Turin, Italy, Nov. 2015.
2. Ammann, M. J. and Z. N. Chen, "Wideband monopole antennas for multi-band wireless systems," *IEEE Trans. Antennas Propag.*, Vol. 45, No. 2, 146–150, Dec. 2003.
3. Luk, K. M. and B. Q. Wu, "The magneto-electric dipole-a wideband antenna for base stations in mobile communications," *Proc. IEEE*, Vol. 100, No. 7, 2297–2307, Jul. 2012.
4. Pan, Y. M., K. W. Leung, and K. Lu, "Compact quasi-isotropic dielectric resonator antenna with small ground plane," *IEEE Trans. Antennas Propag.*, Vol. 62, No. 2, 577–585, Feb. 2014.

5. Wang, D., H. Wong, and C. H. Chan, "Small patch antennas design by substrate integrated irregular ground," *IEEE Trans. Antennas Propag.*, Vol. 60, No. 7, 3096–3103, Jul. 2012.

6. Pazin, L. and Y. Leviatan, "Inverted-F antenna with enhanced bandwidth for WiFi/WiMAX applications," *IEEE Trans. Antennas Propag.*, Vol. 59, No. 3, 1065–1068, Mar. 2011.

7. Sun, J.-S., H.-S. Fang, P.-Y. Lin, and C.-S. Chuang, "Triple-band MIMO antenna for mobile wireless applications," *IEEE Antennas Wireless Propag. Lett.*, Vol. 15, 500–503, Jul. 2015.

8. Lin, D., Z. Y. Lei, Y. J. Xie, G. L. Ning, and J. Fan, "A compact microstrip slot triple-band antenna for WLAN/WiMAX applications," *IEEE Antennas Wireless Propag. Lett.*, Vol. 10, 1178–1181, Dec. 2010.

9. Liu, Y., H.-H. Kim, and H. Kim, "Loop-type ground radiation antenna for dual-band WLAN applications," *IEEE Trans. Antennas Propag.*, Vol. 61, No. 9, 4819–4823, Sep. 2013.

10. Nguyen-Trong, N., A. Piotrowski, and C. Fumeaux, "A frequency-reconfigurable dual-band low-profile monopolar antenna," *IEEE Trans. Antennas Propag.*, Vol. 65, No. 7, 3336–3343, Jul. 2017.

11. Chaouche, Y. B., I. Messaoudene, I. Benmabrouk, M. Nedil, and F. Bouttout, "Compact coplanar waveguide-fed reconfigurable fractal antenna for switchable multiband systems," *IET Microwaves, Antennas Propag.*, Vol. 13, No. 1, 1–8, 2019.

12. Asadallah, F., J. Costantine, and Y. Tawk, "A multiband compact reconfigurable PIFA based on nested slots," *IEEE Antennas Wireless Propag. Lett.*, Vol. 17, No. 2, 331–334, Feb. 2018.

13. Saeed, S. M., C. A. Balanis, and C. R. Birtcher, "Inkjet-printed flexible reconfigurable antenna for conformal WLAN/WiMAX wireless devices," *IEEE Antennas Wireless Propag. Lett.*, Vol. 15, 1979–1982, Mar. 2016.

14. Asif, S. M., M. R. Anbiyaei, K. L. Ford, T. O'Farrell, and R. J. Langley, "Low-profile independently-and concurrently-tunable quad-band antenna for single chain sub-6 GHz 5G new radio applications," *IEEE Access*, Vol. 7, 183770–183782, 2019.

15. Guo, C., L. Deng, J. Dong, T. Yi, C. Liao, S. Huang, and H. Luo, "Variode enabled frequency-reconfigurable microstrip patch antenna with operation band covering S and C bands," *Progress In Electromagnetics Research M*, Vol. 88, 159–167, 2020.